NANO LETTERS

pubs.acs.org/NanoLett Letter

Strain Modulated Superlattices in Graphene

Riju Banerjee,* Viet-Hung Nguyen, Tomotaroh Granzier-Nakajima, Lavish Pabbi, Aurelien Lherbier, Anna Ruth Binion, Jean-Christophe Charlier, Mauricio Terrones, and Eric William Hudson*

Cite This: *Nano Lett.* 2020, 20, 3113−3121 Read Online

ACCESS | Metrics & More | Article Recommendations | Supporting Information

ABSTRACT: Numerous theoretically proposed devices and novel phenomena have sought to take advantage of the intense pseudogauge fields that can arise in strained graphene. Many of these proposals, however, require fields to oscillate with a spatial frequency smaller than the magnetic length, while to date only the generation and effects of fields varying at a much larger length scale have been reported. Here, we describe the creation of short wavelength, periodic pseudogauge-fields using rippled graphene under extreme (>10%) strain and study of its effects on Dirac electrons. Combining scanning tunneling microscopy and atomistic calculations, we find that spatially oscillating strain generates a new quantization different from the familiar Landau quantization. Graphene ripples also cause large variations in carbon−carbon bond length, creating an effective electronic superlattice within a single graphene sheet. Our results thus also establish a novel approach of synthesizing effective 2D lateral heterostructures by periodically modulating lattice strain.

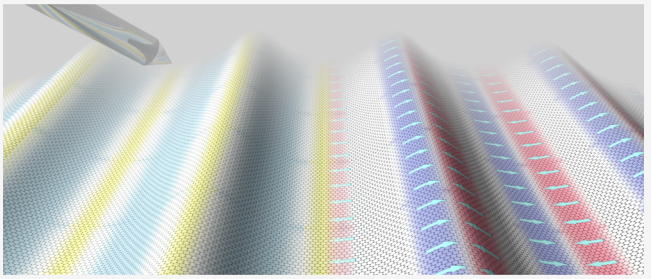

KEYWORDS: *graphene, inhomogeneous strain, superlattice, STM, extreme strain*

Due to its high electronic mobility, optical transparency, mechanical strength, and flexibility, graphene is attractive for electronic applications.[1,2] However, several factors prevent the realization of common electronic applications. For example, the lack of a band gap prevents an effective off-state in graphene transistors. Furthermore, Klein tunneling,[3] in which electrons pass through an electrostatic barrier with perfect transmission, prevents electron confinement by traditional gating methods.

As an alternate means of electronic control, the effects of inhomogeneous magnetic fields on graphene have been theoretically investigated.[4−12] Configurations like square-well magnetic barriers, magnetic dots, and magnetic rings are all predicted to confine electrons in graphene.[6,12] In other cases, where the average B-field is zero, strong resonances that lead to wave vector-[7,8] and valley-[9] filtering are predicted. The physical manifestation of such inhomogeneous magnetic field configurations could lead to new graphene electronic, spintronic and valleytronic devices.[4−10,12]

However, these theoretical proposals have remained unrealized because, unlike the engineering of strong electric field profiles with nanoscale variations, it is difficult to generate large magnetic fields that vary appreciably on the nanometer length scale. Strong magnetic fields created by large magnets are homogeneous at the length scale of most samples. Using presently available techniques like superconducting gates,[13] micromagnets,[14] and gating by ferromagnetic stripes,[15] only weak inhomogeneous fields can be applied to a sample, which were employed to study the behavior of 2D electron gases at the micrometer length scale. As an alternative approach to manipulate Dirac electrons, the application of strain gradients can lead to the emergence of strong pseudogauge fields which manipulate the electronic properties of graphene at the nanoscale.[16] Levy et al.[17] showed that pseudo-Landau levels can be observed in isolated graphene nanobubbles corresponding to locally uniform pseudomagnetic fields of greater than 300 T. However, there the magnetic field strength (measured at the crest of the nanobubble) was relatively uniform and did not vary appreciably over the magnetic length of about 1.5 nm. Such isolated nanobubbles, thus, cannot be used to realize the theoretical proposals of novel electronic, spintronic, and valleytronic devices requiring inhomogeneous fields.[4−10,12] Here, we demonstrate a novel technique to manipulate graphene's electronic properties by periodically modulating lattice strain, creating a superlattice of intense pseudogauge fields that oscillate with a spatial periodicity of a few nanometers, which is comparable to the magnetic length scale.

Pseudogauge potentials arise in graphene due to lattice strain[16,19,20] (Figure 1). As argued by Suzuura and Ando,[19] stretching the graphene lattice changes the local electron

Received: December 11, 2019
Revised: February 25, 2020
Published: March 5, 2020

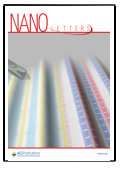

https://dx.doi.org/10.1021/acs.nanolett.9b05108
Nano Lett. 2020, 20, 3113−3121

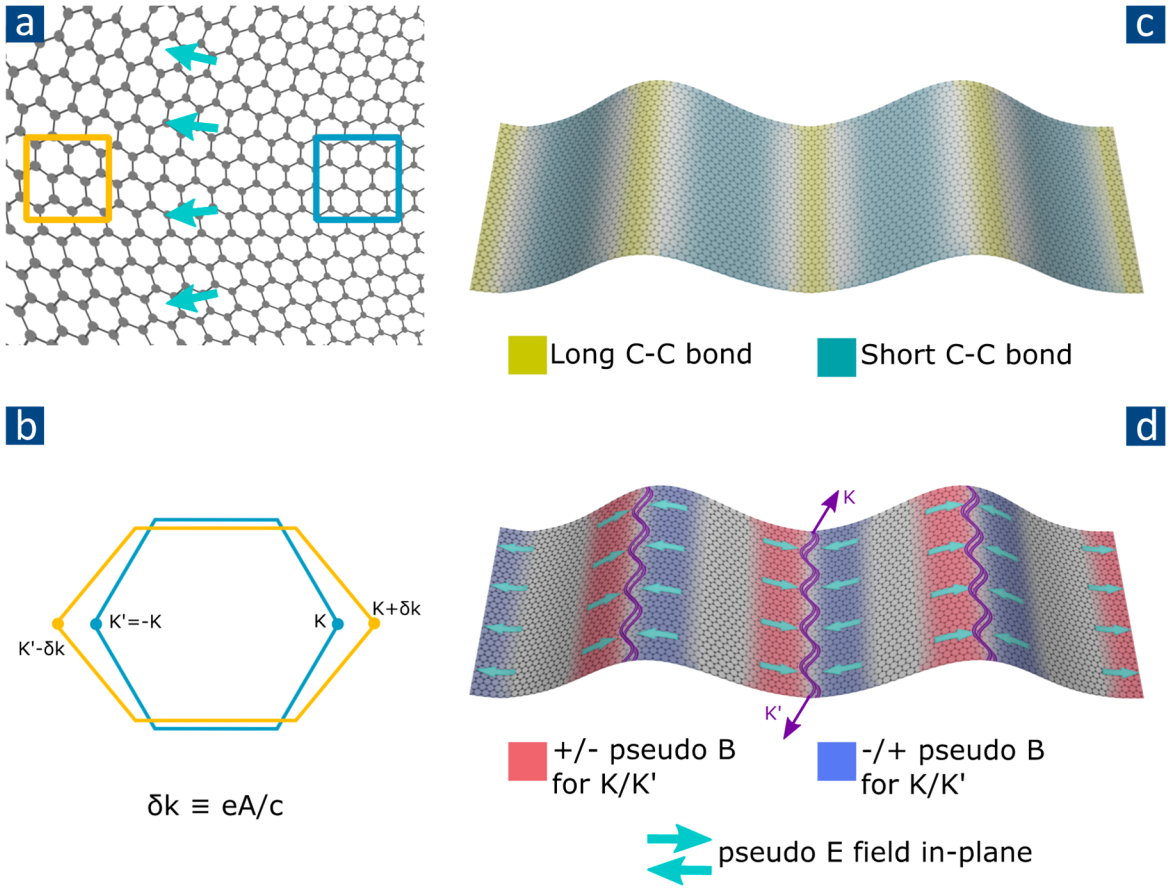

Figure 1. Engineering periodic pseudo-electric and -magnetic fields at strained interfaces: (a) High(low) density of carbon atoms and, hence, electrons are created in regions marked by light-blue (yellow) regions due to a strain gradient. This inhomogeneous charge distribution results in an electric field (green arrows). (b) Stretching of bonds cause the Dirac cones at K and K' points to shift symmetrically (yellow) from their original unstrained positions (light-blue) in the reciprocal space. As a momentum shift δk can be interpreted as generating a pseudovector potential term eA/c[18] (where e is the electronic charge and c is the velocity of light), this creates pseudomagnetic fields with opposite signs at the two valleys. (c) The strain associated with rippling creates rare (yellow) and dense (turquoise) regions in the graphene, effectively acting as two different materials in a superlattice. (d) Pseudofields form near the interfaces of these "materials", both electric (green arrows) and magnetic (red/blue regions indicating the $\pm\hat{z}$ field direction for pseudospin up electrons respectively; pseudospin down are flipped). The up and down magnetic fields are separated by only few nanometers, on the same order as the magnetic length, making the individual Landau levels to interact. LDOS peaks are maximized at the ripple crests and troughs, where valley polarized snake states (violet curved lines) are also expected to form due to the reversal of the pseudospin dependent pseudomagnetic fields across these lines.

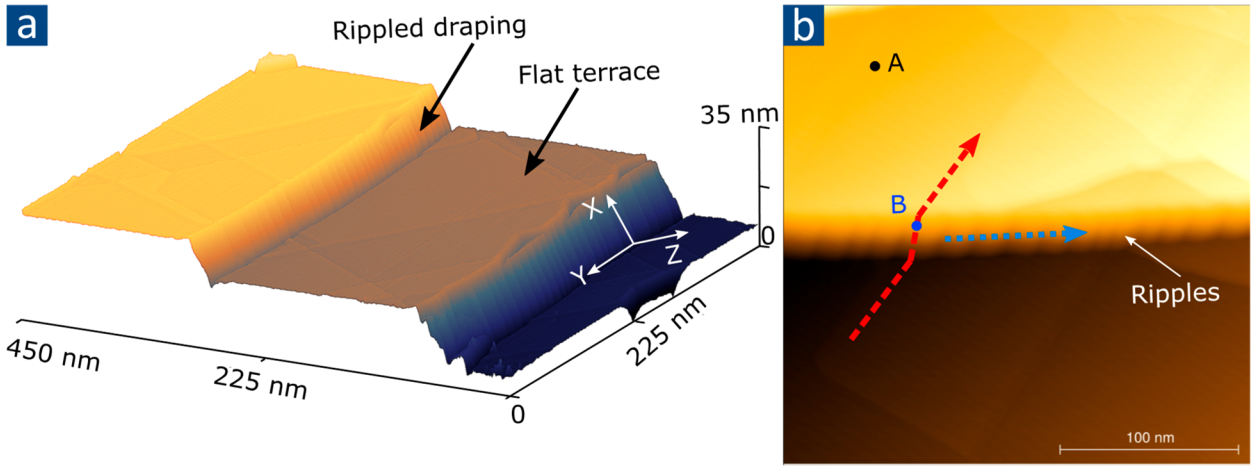

Figure 2. Realizing strain-modulated superlattices: (a) 3D-STM topography of 450 nm square region shows graphene draped over two steps separated by flat terraces. The draped graphene form ripples due to strain. Current set point I_{set} = 62 pA; sample bias V_s = 0.1 V. (b) STM topography zooming in on a step edge, highlighting locations at which data presented in later figures was obtained. I_{set} = 80 pA; V_s = 0.1 V. All topographic data were obtained at T = 80 K and unfiltered.

https://dx.doi.org/10.1021/acs.nanolett.9b05108
Nano Lett. 2020, 20, 3113−3121

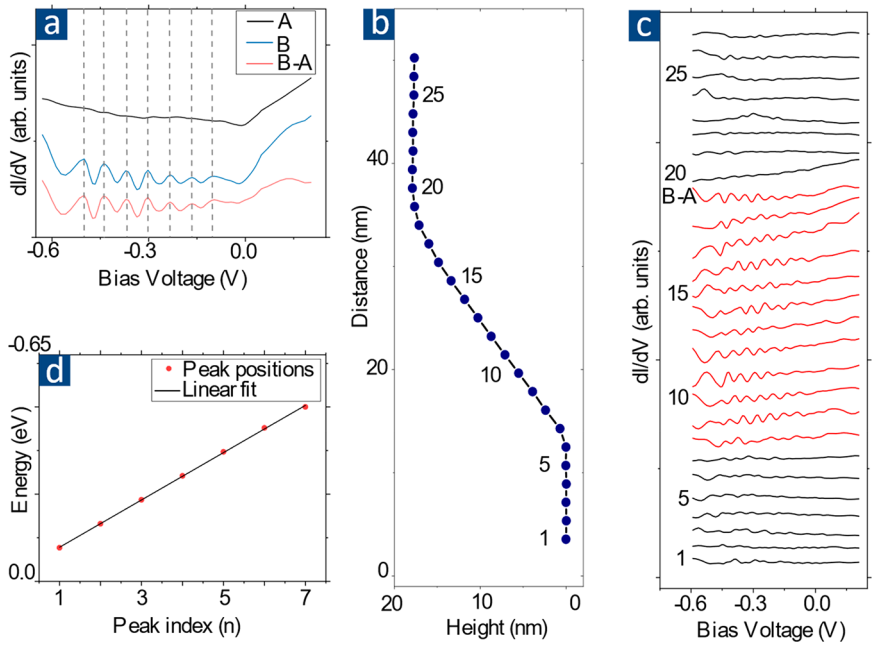

Figure 3. Spectroscopy across a STREMS. (a) Differential conductance spectra taken (A) away from and (B) on a STREMS (locations in Figure 2b). Spectrum (A) has the Dirac point near the Fermi energy ($V = 0$ V). Treating (A) as background, subtraction highlights a series of peaks in the LDOS. Dashed lines aligned with the LDOS peaks are almost equally spaced and are guides to the eye. (b) A line cut rising across the STREMS (along red arrow of Figure 2b) shows that peaks in the background subtracted spectra (c) only appear in the draped region (labeled #8−19, colored red). The Dirac cone shapes of the spectra are suppressed by subtracting the background from each, and the curves are offset for clarity. All these peaks are equally spaced, as shown in (d), plotted for the peaks in spectrum shown in (a), with slope = 67.83(5) meV/peak. For the 12 such spectra in (c), the average slope of energy vs index plots is 69(3) meV/peak. See Supporting Information Sec. 6 for linear fits to all spectra taken on the draped region. All spectra are obtained using standard lock-in techniques, with 13 mV bias modulation at ∼971 Hz.

density which results in an in-plane electric field at the interface of regions with different strains (Figure 1a). Strain also deforms the hexagonal structure in reciprocal space (Figure 1b), moving the Dirac cones at the K and K' points in opposite directions. As changing the momentum $K \rightarrow K + \delta k$ can be interpreted as a pseudo-vector potential,[18] strain gradients also create a pseudomagnetic field perpendicular to the graphene plane.[16] However, unlike an externally applied magnetic field which affects all electrons in a graphene lattice equivalently, the pseudomagnetic field has opposite signs for the K and K' valleys. It has also been shown that the effects of any strain gradient in graphene can be modeled by pseudomagnetic and electric fields.[21−23] It is straightforward to imagine that instead of a uniform strain gradient, which creates uniform pseudogauge fields,[16,19,20] a spatially oscillating strain gradient profile can be used to create a spatially oscillating pseudogauge field profile required to realize the various novel electronic, spintronic, and valleytronic devices discussed earlier.[4−10,12] In this article, we realize such a system by modulating the C−C bond length creating a superlattice of regions which are locally dense and rare (Figure 1c). Alternating zones of oppositely directed pseudogauge fields arise at the interfaces of these regions (Figure 1d). As the magnetic length in each up/down pseudomagnetic field region (colored red and blue in Figure 1d) is comparable to the separation between the two regions, Landau levels in the two regions interact, resulting in a new quantization distinct from the familiar Landau quantization in uniform fields.

To modulate strain in a graphene lattice and realize a pseudogauge field superlattice, we use low-pressure chemical vapor deposition (LPCVD) to grow graphene on electro-polished Cu foils at 1020 °C (see Supporting Information Sec. S1). Previous studies[24] revealed that such high temperatures result in the formation of large Cu steps separated by relatively flat terraces (Figure 2a). We find that graphene sheets grown by this method form continuous films that are pinned on the flat terraces and drape over the large (up to ∼35 nm high) step edges. Upon cooling the sample slowly to 80 K, the draped graphene experiences tensile and shear stresses as it gets pulled by the contact forces of the terraces. This leads to a periodic arrays of ripples, creating a strain enabled modulated superlattice (STREMS), as imaged by a scanning tunneling microscope (STM) (Figure 2a and b).

To demonstrate the emergence of a pseudogauge field superlattice in STREMS, we take differential conductance spectra, representative of the local electronic density of states (LDOS), away from and on top of the ripples (at points A and B in Figure 2b respectively). As shown in Figure 3a, while spectra taken on the terraces (black curve) display the familiar V-shaped Dirac cone,[25] those taken on STREMS (blue curve) reveal a series of peaks. Treating the terrace spectrum as a background, we subtract it to determine the strain-induced spectral modification (red curve). The fact that the strain-induced peaks are confined to the STREMS may be seen in a line-cut (series of spectra) across it (along the red arrow profile in Figure 2b). In Figure 3b and c we plot the height at which the spectra were obtained while climbing the step edge and the background-subtracted spectra, respectively. It is clear from the figures that the LDOS peaks appear only in the spectra from the draped and rippled region (#8−19, colored red). Interestingly, these peaks are equally spaced in energy, scaling as $E_n \propto n$ (Figure 3d). In addition to this energy dependence of the peaks, we also find a spatially periodic modulation of their amplitude, as shown in a line-cut along the STREMS (Figure

https://dx.doi.org/10.1021/acs.nanolett.9b05108
Nano Lett. 2020, 20, 3113−3121

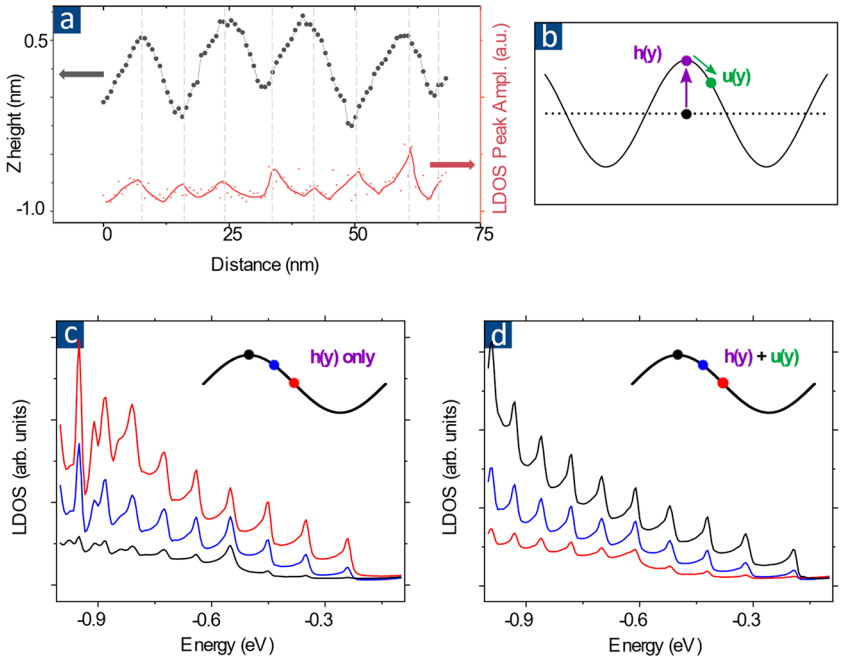

Figure 4. Average LDOS peak amplitude along the ripple. (a) A line cut along the ripple (blue arrow in Figure 2b) reveals that the amplitude of LDOS peaks (red) is maximized at the crests and troughs of the nearly triangular ripples (black). All lines are guides to the eye. (b) Displacement (out-of-plane $h(y)$ and in-plane $u(y)$) fields to be considered in rippled graphene. Simulated LDOS as a function of electron energy obtained when only out-of-plane displacements are considered (c) and when in-plane displacements are added (d) show that in-plane displacements are necessary to match the experimental results. Simulations calculated using displacement parameters λ = 20 nm, h_0 = 2.5 nm, and u_0 = 3.5 Å.

2b, blue arrow). In Figure 4a we show that the amplitude of the LDOS peaks (red curve) is closely tied to the z-height profile (black curve), peaking at the ripple crests and troughs of the triangular ripples.

We note that these LDOS peaks are superficially similar to those found in a variety of previous STM measurements of locally strained (e.g., wrinkled or bubbled) graphene,[17,22,26,27] where the LDOS is associated with Landau levels arising from strain-induced uniform pseudomagnetic fields. However, unlike our observed linear scaling (implying $E_n \propto n$, in Figure 3d), the energies of those peaks were reported[17,22,26,27] to scale as $E_n \propto \sqrt{n}$. Previous studies have observed equally spaced peaks in LDOS spectra in graphene and attributed them to confinement effects.[28] While it is possible to confine graphene electrons by strain,[29,30] we discard that as a feasible explanation of our observed LDOS peaks as contrary to confinement peaks, the energy gap between our LDOS peaks remains unchanged for spectra taken on ripples with very different wavelengths (see Supporting Information Sec. S2).

To clarify the origin of our LDOS peaks, atomistic calculations based on a p_z tight-binding Hamiltonian with nearest neighbor couplings were performed with $H_{tb} = \sum_{\langle n,m\rangle} t_{nm} c_n^{\dagger} c_m$, where the hopping energies t_{nm} are determined as a function of the C−C bond length r_{nm}:[31]

$$t_{nm} = t_0 \exp\left[-\beta\left(\frac{r_{nm}}{r_0} - 1\right)\right] \quad (1)$$

where t_0 = −2.6 eV and r_0 = 1.42 Å were used as the corresponding parameters for unstrained graphene. The decay rate β was adjusted to 4.5 by fitting first-principles calculations, while a value of 3.37 is usually used in flat graphene systems with in-plane deformations only.[31] Due to the exponential dependence of the hopping energy on the bond length r_{nm}, eq 1 implies that even a small change in r_{nm} can have significant effects in modifying the local electronic properties. See Supporting Information Sec. S3 for more details about the calculations and the reason to require this modification in β.

To understand the profile of mechanical deformations, we consider a graphene sheet stretched under a constant tensile strain along the x-axis (axes directions are defined in Figure 2a). A sinusoidal strain profile with out-of-plane displacements $h(y) = h_0 \sin\left(2\pi\frac{y}{\lambda}\right)$, with λ being the ripple wavelength, is then used to emulate the periodic ripples along the y-axis. In addition, curvature at the crests and troughs can also result in an in-plane displacement profile which can be modeled by a strain profile $u_y(y) = u_0 \sin\left(4\pi\frac{y}{\lambda}\right)$. The two displacement profiles (out-of-plane and in-plane) are shown in Figure 4b. The two different displacement profiles can be used to describe two significantly different modes of deformations which can occur in a ripple. For a given displacement profile $h(y) + u_y(y)$, when u_0 is sufficiently small (or zero), a strain profile is obtained with small C−C bond lengths at the ripple crests and troughs and larger C−C bond lengths in the regions in between. However, for large enough u_0, the opposite situation occurs—describing a deformation profile with large C−C bond lengths at the crests and troughs and smaller C−C bond lengths in between. Although this simple model does not exactly reproduce the triangular shape of ripples observed experimentally, varying these two displacement fields allows us to investigate various deformation profiles and provides insights required to identify the model which agrees well with experimentally measured values.

Simulated LDOS obtained for the two situations discussed above (without and with in-plane displacements) are presented in Figure 4c and d, respectively. In both cases (Figure 4c and d), we observe that a periodic strain profile described by $h(y)$

https://dx.doi.org/10.1021/acs.nanolett.9b05108
Nano Lett. 2020, 20, 3113−3121

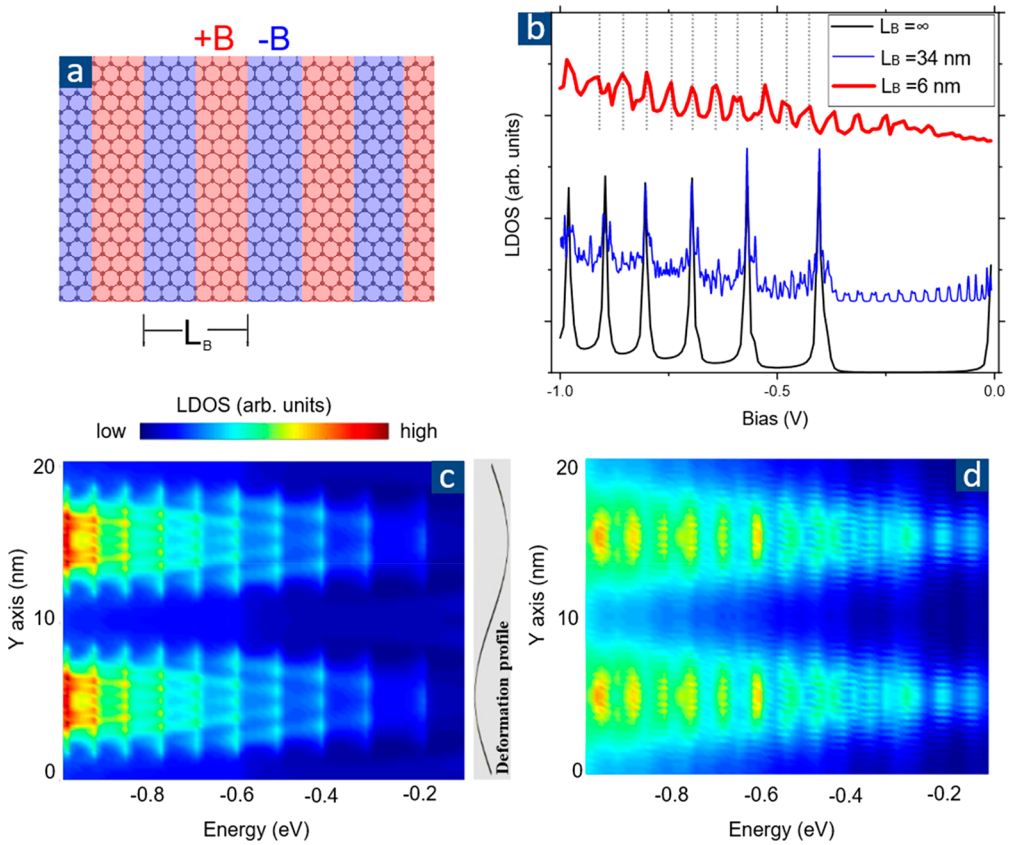

Figure 5. DOS in periodic gauge fields: (a) A model system of Dirac electrons in alternating magnetic field directions with periodicity L_B is used to understand our experimental LDOS. (b) The calculated DOS for different values of L_B. The black curve, corresponding to $L_B \to \infty$ corresponds to the case of standard Landau quantization with energy peaks at $E_n \propto \sqrt{n}$. However, as the periodicity is reduced (blue curve), the spectra deviates from the standard Landau picture with more features. When the periodicity L_B is reduced further and made of the same order of magnitude as the magnetic length, the DOS (red curve) is drastically different from the Landau quantized states (black curve). The peaks in the red curve are almost equally spaced, as observed in our experiments. All calculations in (b) are done with $|B|$ = 160 T. The plots are offset for clarity. Equally spaced dashed lines are guides to the eye. (c, d) Theoretical calculations reproducing the observed spatial variation of these quantized states. Both (c) strained and (d) unstrained + pseudopotential tight binding models capture important features in spectroscopy obtained along the ripple (blue arrow in Figure 2b). LDOS peaks are almost equally spaced in energy, as observed in Figure 3d. The LDOS amplitudes are higher at the crests and troughs of the ripples, as observed in Figure 4a. The simulation also captures the feature of having higher LDOS weight at large negative biases, as observed in Figure 3a.

and $u_y(y)$ results in a series of almost equally spaced LDOS peaks, similar to our experimental observations (Figure 3a, blue curve). The weakly varying peak spacing in the simulated LDOS (of ∼80 meV) is also consistent with the experimentally observed peak spacing of 69(3) meV (in Figure 3a, c, and d); the small difference attributable to the fact that the simulation estimates the deformation profile as sinusoidal functions, instead of the observed triangular ripples. This is in stark contrast to a multitude of previous studies[17,22,26,27] where uniform strain gradients resulted in LDOS peaks corresponding to $E_n \propto \sqrt{n}$. More interestingly, while both models yield equally spaced LDOS peaks, the spatial variation of the amplitudes of those peaks is model dependent. In Figure 4c, where we consider the out-of-plane displacement $h(y)$ only, higher amplitude peaks occur in the region between the crests and troughs of the ripples. In contrast, in Figure 4d, where we consider both out-of-plane and in-plane displacement profiles ($h(y)$ and $u_y(y)$), higher amplitude peaks occur at the crests and troughs. As the latter (Figure 4d) is consistent with our measurements (Figure 4a), in-plane displacement must be included ($u_y(y) \neq 0$) in our calculations, implying that both displacement fields $h(y) + u_y(y)$ concurrently occur and play a major role in determining the electronic properties of rippled graphene. Many theoretical studies have treated out-of-plane and in-plane deformation of graphene independently.[30,32−35] Figure 4 refutes such an assumption as both deformations occur concurrently and are significant enough to modify the local electronic properties. We also note that significant in-plane stretching was crucial in explaining the mechanical properties of the same system.[36]

While the strain profile of ripples can be deciphered from measuring the local electronic properties and fitting it to a theoretical model, such a periodic oscillation of atomic displacements is very difficult to directly image using microscopy techniques. Though atoms can be imaged, extracting an accurate value of strain over a very narrow region at the crests and troughs by measuring individual atomic displacements of a few percent of the C−C bond length is challenging. So, to demonstrate that strain varies at the crests and troughs of the ripples, we took the indirect route of measuring resultant electronic properties ($E_n \propto n$ with higher LDOS weight at the crests and troughs) and fitting it to a theoretical model (detailed in Figure 4). The local electronic properties can be measured much more accurately (as each

https://dx.doi.org/10.1021/acs.nanolett.9b05108
Nano Lett. 2020, 20, 3113−3121

spectrum is averaged 150 times), which enables us to do a more thorough analysis than measuring atomic displacements.

Next, we turn to our observation of equally spaced ($E_n \propto n$) LDOS peaks (Figure 3d) as opposed to $E_n \propto \sqrt{n}$ peaks in previous studies of strained graphene.[17,22,26,27] Under the effect of a spatially uniform magnetic field, Dirac electrons settle into Landau levels with $E_n \propto \sqrt{n}$ quantization. A crucial component of this familiar Landau quantization is the spatial uniformity of the magnetic field. The electronic quantization deviates from the familiar Landau quantization for spatially nonuniform magnetic field profiles. To illustrate this point, we show the DOS of a model system of Dirac electrons under a spatially periodic magnetic field profile with periodicity L_B (Figure 5a). In the limit $L_B \rightarrow \infty$, the DOS corresponds to standard Landau quantization with $E_n \propto \sqrt{n}$ (black curve in Figure 5b). However, as the periodicity L_B is reduced (blue curve in Figure 5b, corresponding to $L_B = 34$ nm), quantum Hall edge states are formed in each uniform B-field zones but propagate oppositely in zones of opposite B-fields. As the electrons are forced to circulate along the edges of the constant field zones, they pick up a phase (Aharonov−Bohm phase) causing them to interfere,[37] as electrons circulating around opposite B-field zones pick up opposite phases. The interference between these opposite propagating Hall states at the interface between zones of opposite B-fields modifies the quantization picture. In addition to the high DOS peaks corresponding to the standard Landau quantization, many smaller DOS peaks are observed in the blue curve in Figure 5b. These small DOS peaks are essentially due to the aforementioned interaction between opposite propagating states that can induce the interference effects as investigated in a recent calculation by Nguyen and Charlier.[38] On reducing the periodicity further (red curve in Figure 5b) and making L_B the same order of magnitude as the magnetic length, the DOS profile is drastically different from the Landau quantized states. The red curve shows peaks which are almost equally spaced as observed in our experiments. Thus, we interpret our observation of $E_n \propto n$ LDOS peaks as a direct consequence of having a spatially oscillating magnetic field profile. Previous studies of strained graphene have reported the emergence of pseudogauge fields in structures like nanobubbles[17] and wrinkles[26,39,40] where the pseudomagnetic field has been constant over a length scale much larger than the magnetic length. The fact that there are no experimental works yet detailing the results of inhomogeneous pseudomagnetic fields is because, prior to the present work, inhomogeneous field profiles have not been created with any regularity to make the system amenable enough for thorough experimental and theoretical explorations. We also present an analytical derivation showing the emergence of $E_n \propto n$ quantization for Dirac electrons under a periodic magnetic field profile in the Supporting Information Sec. S7. Note that the above analysis is independent of the orientation of the graphene sheet with respect to the direction of the periodicity of the magnetic field. Similar experimental observations like the ones reported were made on different step edges which curve significantly, proving the fact that a pseudogauge field superlattice is formed by a periodic strain profile irrespective of the small details like orientation of the graphene with respect to the Cu substrate and periodicity of the magnetic field.

A further demonstration of the emergence of spatially periodic pseudomagnetic and electric fields in our rippled graphene system is presented in Figure 5c and d. We consider an effective model of unstrained flat graphene with a tight binding Hamiltonian, pseudomagnetic field $\vec{B}_S = B_{max} \sin\left(4\pi\frac{y}{\lambda}\right)\vec{e}_z$ and electric potential $V_S = V_{max} \cos\left(4\pi\frac{y}{\lambda}\right)$, and compare it to a strained tight-binding model using the deformation profile discussed earlier (with both out-of-plane and in-plane deformations). LDOS maps from these two models are displayed in Figure 5d and c, respectively. The result obtained from an unstrained model with only including the combined effects of spatially varying E- and B- fields (Figure 5d) is in good qualitative agreement with that obtained in the periodically strained system (Figure 5c). This implies that both pseudomagnetic and electric fields are induced by the corresponding strain field and play significant roles in influencing the electronic properties of the system. For a more detailed explanation for the requirement of pseudo-electric fields in addition to pseudomagnetic fields, and to explain the spatial variation of the observed spectra, see the Supporting Information Sec. S4.

The above investigations confirm the generation of strain modulated superlattices, as displayed in Figure 1c, d. We apply extreme strain to a graphene sheet, measuring over 10% as both estimated from our simulated models (Supporting Information Sec. S3) and measured directly by imaging the graphene lattice (Supporting Information Sec. S5). Analogous to a classical fabric under stress in the longitudinal direction, graphene ripples in the transverse direction to form ripples, creating a spatially varying strain profile. The periodic spatial variation of this strain modulates the C−C bonds in graphene, creating a superlattice of regions which are locally dense (turquoise, with short C−C bonds) and rare (yellow, with long C−C bonds) (Figure 1c). Pseudopotentials arise from this strain profile as do associated pseudogauge fields, as illustrated in Figure 1d. The pseudogauge fields, which are spatial derivatives of the potentials, become large in the presence of strain gradients and are hence maximized at the interfaces between dense and rare regions. From tight-binding calculations employing a sinusoidal strain profile, we find that $B_{max} \sim 100$ T and $E_{max} \sim 10^7$ V/m are required to match the experimental measurements. In analogy to traditional superlattices, where novel electronic states emerge at the interfaces of two different materials, quantized energy spectra arise due to the combined effects of interfacial oscillating pseudo (B, E) fields.

The values for B_{max} and E_{max} determined here from atomistic calculations may be underestimated as the experimentally determined ripple shape is found to better resemble a triangular waveform, characterized by sharp crests and troughs. This would indicate a much larger strain gradient in our system relative to a sinusoidal waveform used to estimate the deformation profile and therefore possibly much larger pseudogauge fields than those predicted by the model. We also note that the LDOS peaks in Figure 3c do not line up exactly. This is likely because of small variations of the strain magnitude along the line on which spectra are taken. Along that line, the strain magnitudes as characterized by parameters $h(y)$ (out-of-plane displacement) and $u_y(y)$ (in-plane displacement) will vary. As discussed in the earlier, $h(y)$ and $u_y(y)$ are maximum at the crests and troughs of the ripples. It is difficult to take spectra along a line where both $h(y)$ and $u_y(y)$ parameters are absolutely constant, and hence, some strain variation is observed in the spectra and their peak positions do

https://dx.doi.org/10.1021/acs.nanolett.9b05108
Nano Lett. 2020, 20, 3113−3121

not line up. We also observe significant electron−hole asymmetry in our spectra, as the equally spaced peaks (Figure 3a, c) are seen only at negative biases. Such asymmetry was found by Bai et al.[41] to be arising from enhanced next-nearest neighbor hopping due to strain induced lattice deformations. Electron−hole asymmetry on the flat terraces (Figure 3a, black curve) with higher DOS at positive biases is frequently observed for graphene grown on metallic substrates like Cu[42] or Ag.[43]

We also note that as rendered in Figure 1d (by violet curved lines), alternating zones of oppositely directed pseudomagnetic fields should also lead to the formation of oppositely propagating valley−Hall edge states.[16,44,45,38] These edge states can represent snake-like trajectories[46] at the interfaces between zones of opposite pseudomagnetic fields.[47−49] Since the direction of these magnetic fields is valley dependent,[16,19,20] our graphene ripples can also be a potential candidate for exploring valley dependent transport phenomena.[9,47,50] In our measurements, the spectral signatures of the snake states are seen in an increased intensity of the LDOS peaks at the ripple crests and troughs (Figure 4a).

With our realization of pseudogauge fields which are simultaneously intense (∼100 T) and modulated at short length scales (∼1−10 nm), we can finally begin to realize theoretical proposals of valley filters and electron optics in graphene which require localized magnetic barriers.[4−8,10−12] It will also be interesting to explore the consequences of such strain profiles in a wide variety of 2D materials which should also support STREMS and where strain is known to significantly influence electronic properties.[51−55] The intensity of these inhomogeneous pseudofields should make realization of these proposals possible even at room temperatures.[17,56]

Note: When the paper was in review, we came to know about another paper by Jiang et al.[57] where periodically strained superlattices were created in graphene by placing it on $NbSe_2$.

■ ASSOCIATED CONTENT

Supporting Information

The Supporting Information is available free of charge at https://pubs.acs.org/doi/10.1021/acs.nanolett.9b05108.

Methods, details of the sample growth, negating other possible origins of the data, details of theoretical calculations, strain measurements, $E_n \propto n$ plots, Toy model for Dirac electrons in inhomogeneous magnetic fields, and surface reconstruction of the Cu substrate (PDF)

■ AUTHOR INFORMATION

Corresponding Authors

Eric William Hudson − *Department of Physics, The Pennsylvania State University, University Park, Pennsylvania 16802, United States*; Email: ehudson@psu.edu

Riju Banerjee − *Department of Physics, The Pennsylvania State University, University Park, Pennsylvania 16802, United States*; orcid.org/0000-0003-3454-6960; Email: riju@psu.edu

Authors

Viet-Hung Nguyen − *Institute of Condensed Matter and Nanosciences, Université Catholique de Louvain, B-1348 Louvain-la-Neuve, Belgium*

Tomotaroh Granzier-Nakajima − *Department of Physics, The Pennsylvania State University, University Park, Pennsylvania 16802, United States*

Lavish Pabbi − *Department of Physics, The Pennsylvania State University, University Park, Pennsylvania 16802, United States*

Aurelien Lherbier − *Institute of Condensed Matter and Nanosciences, Université Catholique de Louvain, B-1348 Louvain-la-Neuve, Belgium*

Anna Ruth Binion − *Department of Physics, The Pennsylvania State University, University Park, Pennsylvania 16802, United States*

Jean-Christophe Charlier − *Institute of Condensed Matter and Nanosciences, Université Catholique de Louvain, B-1348 Louvain-la-Neuve, Belgium*

Mauricio Terrones − *Department of Physics, The Pennsylvania State University, University Park, Pennsylvania 16802, United States*; orcid.org/0000-0003-0010-2851

Complete contact information is available at: https://pubs.acs.org/10.1021/acs.nanolett.9b05108

Author Contributions

R.B. conceived the project. R.B. and L.P. built the custom instrument. T.G.N. prepared the samples. R.B. and L.P. collected the data. R.B. performed analysis. R.B., V.H.N., and A.L. performed theoretical modeling. All authors took part in interpreting the results. R.B., V.H.N., T.G.N., A.L., J.-C.C, M.T., and E.W.H. wrote the paper. J.C.C., M.T., and E.W.H. advised.

Funding

This material is based upon work supported by the National Science Foundation (1229138). T.G.N. and M.T. acknowledge The Air Force Office of Scientific Research (AFOSR) (17RT0244) for financial support. V.-H.N., A.L., and J.-C.C. acknowledge financial support from the Francqui Foundation and the F.R.S.-FNRS of Belgium through a research project (T.1077.15), from the Flag-Era JTC 2017 project "MECHANIC" (R.50.07.18.F), from the Fédération Wallonie-Bruxelles through the ARC on 3D nanoarchitecturing of 2D crystals (16/21-077), and from the European Union's Horizon 2020 research and innovation program (696656).

Notes

The authors declare no competing financial interest.

■ ACKNOWLEDGMENTS

We thank J.A. Stroscio, J. Hoffman, V. Crespi, and J.K. Jain for helpful discussions.

■ REFERENCES

(1) Geim, A. K.; Novoselov, K. S. The rise of graphene. *Nat. Mater.* **2007**, *6*, 183−191.

(2) Castro Neto, A. H.; Guinea, F.; Peres, N. M. R. R.; Novoselov, K. S.; Geim, A. K. The electronic properties of graphene. *Rev. Mod. Phys.* **2009**, *81*, 109−162.

(3) Katsnelson, M. I.; Novoselov, K. S.; Geim, A. K. Chiral tunnelling and the Klein paradox in graphene. *Nat. Phys.* **2006**, *2*, 620.

(4) Tan, L. Z.; Park, C.-H.; Louie, S. G. Graphene Dirac fermions in one-dimensional inhomogeneous field profiles: Transforming magnetic to electric field. *Phys. Rev. B: Condens. Matter Mater. Phys.* **2010**, *81*, 195426.

(5) Ramezani Masir, M.; Vasilopoulos, P.; Peeters, F. M. Fabry-Perot resonances in graphene microstructures: Influence of a magnetic field. *Phys. Rev. B: Condens. Matter Mater. Phys.* **2010**, *82*, 115417.

(6) De Martino, A.; Dell'Anna, L.; Egger, R. Magnetic Confinement of Massless Dirac Fermions in Graphene. *Phys. Rev. Lett.* **2007**, *98*, No. 066802.
(7) Ramezani Masir, M.; Vasilopoulos, P.; Matulis, A.; Peeters, F. M. Direction-dependent tunneling through nanostructured magnetic barriers in graphene. *Phys. Rev. B: Condens. Matter Mater. Phys.* **2008**, *77*, 235443.
(8) Dell'Anna, L.; De Martino, A. Multiple magnetic barriers in graphene. *Phys. Rev. B: Condens. Matter Mater. Phys.* **2009**, *79*, No. 045420.
(9) Wu, Z.; Zhai, F.; Peeters, F. M.; Xu, H. Q.; Chang, K. Valley-Dependent Brewster Angles and Goos-Hänchen Effect in Strained Graphene. *Phys. Rev. Lett.* **2011**, *106*, 176802.
(10) Ghosh, S.; Sharma, M. Electron optics with magnetic vector potential barriers in graphene. *J. Phys.: Condens. Matter* **2009**, *21*, 292204.
(11) Ramezani Masir, M; Vasilopoulos, P; Peeters, F M Kronig–Penney model of scalar and vector potentials in graphene. *J. Phys.: Condens. Matter* **2010**, *22*, 465302.
(12) Ramezani Masir, M; Vasilopoulos, P; Peeters, F M Graphene in inhomogeneous magnetic fields: bound, quasi-bound and scattering states. *J. Phys.: Condens. Matter* **2011**, *23*, 315301.
(13) Geim, A. K.; Dubonos, S. V.; Grigorieva, I. V.; Bending, S. J. Size-scaling experiment in a two-dimensional electron gas using an inhomogeneous magnetic field due to a superconducting gate. *Surf. Sci.* **1996**, *361–362*, 311–314.
(14) Ye, P. D.; et al. Electrons in a Periodic Magnetic Field Induced by a Regular Array of Micromagnets. *Phys. Rev. Lett.* **1995**, *74*, 3013–3016.
(15) Izawa, S.; Katsumoto, S.; Endo, A.; Iye, Y. Magnetoresistance Oscillation in Two-Dimensional Electron Gas under Spatially Modulated Vector Potential. *J. Phys. Soc. Jpn.* **1995**, *64*, 706–710.
(16) Guinea, F.; Katsnelson, M. I.; Geim, A. K. Energy gaps and a zero-field quantum Hall effect in graphene by strain engineering. *Nat. Phys.* **2010**, *6*, 30–33.
(17) Levy, N.; et al. Strain-Induced Pseudo–Magnetic Fields Greater Than 300 T in Graphene Nanobubbles. *Science* **2010**, *329*, 544–547.
(18) Goldstein, H.; Poole, C. P.; Safko, J. L. *Classical Mechanics*, 3rd ed.; Addison-Wesley: San Francisco, CA 2002.
(19) Suzuura, H.; Ando, T. Phonons and electron-phonon scattering in carbon nanotubes. *Phys. Rev. B: Condens. Matter Mater. Phys.* **2002**, *65*, 1.
(20) Shioya, H.; Russo, S.; Yamamoto, M.; Craciun, M. F.; Tarucha, S. Electron States of Uniaxially Strained Graphene. *Nano Lett.* **2015**, *15*, 7943–7948.
(21) Guinea, F.; Horovitz, B.; Le Doussal, P. Gauge field induced by ripples in graphene. *Phys. Rev. B: Condens. Matter Mater. Phys.* **2008**, *77*, 205421.
(22) Liu, Y.; et al. Tailoring sample-wide pseudo-magnetic fields on a graphene–black phosphorus heterostructure. *Nat. Nanotechnol.* **2018**, *13*, 828.
(23) Qi, Z.; et al. Pseudomagnetic fields in graphene nanobubbles of constrained geometry: A molecular dynamics study. *Phys. Rev. B: Condens. Matter Mater. Phys.* **2014**, *90*, 125419.
(24) Yi, D.; et al. What Drives Metal-Surface Step Bunching in Graphene Chemical Vapor Deposition? *Phys. Rev. Lett.* **2018**, *120*, 246101.
(25) Rutter, G. M.; et al. Scattering and Interference in Epitaxial Graphene. *Science* **2007**, *317*, 219–222.
(26) Meng, L.; et al. Strain-induced one-dimensional Landau level quantization in corrugated graphene. *Phys. Rev. B: Condens. Matter Mater. Phys.* **2013**, *87*, 205405.
(27) Jiang, Y.; et al. Visualizing Strain-Induced Pseudomagnetic Fields in Graphene through an hBN Magnifying Glass. *Nano Lett.* **2017**, *17*, 2839–2843.
(28) Jiang, Y.; et al. Tuning a circular p–n junction in graphene from quantum confinement to optical guiding. *Nat. Nanotechnol.* **2017**, *12*, 1045–1049.
(29) Carrillo-Bastos, R.; Faria, D.; Latgé, A.; Mireles, F.; Sandler, N. Gaussian deformations in graphene ribbons: Flowers and confinement. *Phys. Rev. B: Condens. Matter Mater. Phys.* **2014**, *90*, No. 041411.
(30) Wu, Y.; et al. Quantum Wires and Waveguides Formed in Graphene by Strain. *Nano Lett.* **2018**, *18*, 64–69.
(31) Pereira, V. M.; Castro Neto, A. H.; Peres, N. M. R. Tight-binding approach to uniaxial strain in graphene. *Phys. Rev. B: Condens. Matter Mater. Phys.* **2009**, *80*, No. 045401.
(32) Lu, Q.; Huang, R. NONLINEAR MECHANICS OF SINGLE-ATOMIC-LAYER GRAPHENE SHEETS. *Int. J. Appl. Mechanics* **2009**, *01*, 443–467.
(33) Zhang, D.-B.; Akatyeva, E.; Dumitrică, T. Bending Ultrathin Graphene at the Margins of Continuum Mechanics. *Phys. Rev. Lett.* **2011**, *106*, 255503.
(34) Wei, Y.; Wang, B.; Wu, J.; Yang, R.; Dunn, M. L. Bending Rigidity and Gaussian Bending Stiffness of Single-Layered Graphene. *Nano Lett.* **2013**, *13*, 26–30.
(35) Lu, Q.; Arroyo, M.; Huang, R. Elastic bending modulus of monolayer graphene. *J. Phys. D: Appl. Phys.* **2009**, *42*, 102002.
(36) Banerjee, R.; Granzier-Nakajima, T.; Pabbi, L.; Terrones, M.; Hudson, E. W. Atomically sharp non-classical ripples in graphene. *arXiv:1912.11732 [cond-mat]*; arXiv: 2019; https://arxiv.org/abs/1912.11732 (accessed 2020-3-3).
(37) de Juan, F.; Cortijo, A.; Vozmediano, M. A. H.; Cano, A. Aharonov–Bohm interferences from local deformations in graphene. *Nat. Phys.* **2011**, *7*, 810–815.
(38) Nguyen, V. H.; Charlier, J.-C. Stepped graphene-based Aharonov–Bohm interferometers. *2D Mater.* **2019**, *6*, No. 045045.
(39) Tapasztó, L.; et al. Breakdown of continuum mechanics for nanometre-wavelength rippling of graphene. *Nat. Phys.* **2012**, *8*, 739–742.
(40) Teague, M. L.; et al. Evidence for Strain-Induced Local Conductance Modulations in Single-Layer Graphene on SiO2. *Nano Lett.* **2009**, *9*, 2542–2546.
(41) Bai, K.-K.; et al. Detecting giant electron-hole asymmetry in a graphene monolayer generated by strain and charged-defect scattering via Landau level spectroscopy. *Phys. Rev. B: Condens. Matter Mater. Phys.* **2015**, *92*, 121405.
(42) Bai, K.-K.; et al. Generating atomically sharp p–n junctions in graphene and testing quantum electron optics on the nanoscale. *Phys. Rev. B: Condens. Matter Mater. Phys.* **2018**, *97*, No. 045413.
(43) Kiraly, B.; Iski, E. V.; Mannix, A. J.; Fisher, B. L.; Hersam, M. C.; Guisinger, N. P. Solid-source growth and atomic-scale characterization of graphene on Ag(111). *Nat. Commun.* **2013**, *4*, 1–7.
(44) Ramezani Masir, M; Vasilopoulos, P; Peeters, F M Magnetic Kronig–Penney model for Dirac electrons in single-layer graphene. *New J. Phys.* **2009**, *11*, No. 095009.
(45) Kormányos, A.; Rakyta, P.; Oroszlány, L.; Cserti, J. Bound states in inhomogeneous magnetic field in graphene: Semiclassical approach. *Phys. Rev. B: Condens. Matter Mater. Phys.* **2008**, *78*, 1.
(46) Evers, F.; Mirlin, A. D.; Polyakov, D. G.; Wölfle, P. Semiclassical theory of transport in a random magnetic field. *Phys. Rev. B: Condens. Matter Mater. Phys.* **1999**, *60*, 8951–8969.
(47) Settnes, M.; Power, S. R.; Brandbyge, M.; Jauho, A.-P. Graphene Nanobubbles as Valley Filters and Beam Splitters. *Phys. Rev. Lett.* **2016**, *117*, 276801.
(48) Ghosh, T. K.; De Martino, A.; Häusler, W.; Dell'Anna, L.; Egger, R. Conductance quantization and snake states in graphene magnetic waveguides. *Phys. Rev. B: Condens. Matter Mater. Phys.* **2008**, *77*, No. 081404.
(49) Oroszlány, L.; Rakyta, P.; Kormányos, A.; Lambert, C. J.; Cserti, J. Theory of snake states in graphene. *Phys. Rev. B: Condens. Matter Mater. Phys.* **2008**, *77*, 1.
(50) Jones, G. W.; Bahamon, D. A.; Castro Neto, A. H.; Pereira, V. M. Quantized Transport, Strain-Induced Perfectly Conducting Modes, and Valley Filtering on Shape-Optimized Graphene Corbino Devices. *Nano Lett.* **2017**, *17*, 5304–5313.

https://dx.doi.org/10.1021/acs.nanolett.9b05108
Nano Lett. 2020, 20, 3113–3121

(51) Naumis, G. G.; Barraza-Lopez, S.; Oliva-Leyva, M.; Terrones, H. Electronic and optical properties of strained graphene and other strained 2D materials: a review. *Rep. Prog. Phys.* **2017**, *80*, No. 096501.
(52) Okada, Y.; et al. Visualizing Landau Levels of Dirac Electrons in a One-Dimensional Potential. *Phys. Rev. Lett.* **2012**, *109*, 166407.
(53) Zeljkovic, I.; et al. Strain engineering Dirac surface states in heteroepitaxial topological crystalline insulator thin films. *Nat. Nanotechnol.* **2015**, *10*, 849−853.
(54) Wei, W.; Dai, Y.; Huang, B. Straintronics in two-dimensional in-plane heterostructures of transition-metal dichalcogenides. *Phys. Chem. Chem. Phys.* **2017**, *19*, 663−672.
(55) Akinwande, D.; et al. A review on mechanics and mechanical properties of 2D materials—Graphene and beyond. *Extreme Mechanics Letters* **2017**, *13*, 42−77.
(56) Nigge, P.; et al. Room temperature strain-induced Landau levels in graphene on a wafer-scale platform. *Science Advances* **2019**, *5*, No. eaaw5593.
(57) Jiang, Y. et al. Flat Bands in Buckled Graphene Superlattices. *arXiv:1904.10147[cond-mat]*; arXiv: 2019; https://arxiv.org/abs/1904.10147 (accessed 2020-3-3).

https://dx.doi.org/10.1021/acs.nanolett.9b05108
Nano Lett. 2020, 20, 3113−3121